Hindawi
International Transactions on Electrical Energy Systems
Volume 2023, Article ID 8950650, 14 pages
https://doi.org/10.1155/2023/8950650

Research Article

Modified Differential Evolution Algorithm for Governing Virtual Inertia of an Isolated Microgrid Integrating Electric Vehicles

Debayani Mishra,[1,2] **Manoj Kumar Maharana**,[2] **Manoj Kumar Kar**,[3] **Anurekha Nayak**,[4] **and Murthy Cherukuri**[5]

[1]*Ajay Binay Institute of Technology, Cuttack, India*
[2]*KIIT Deemed to be University, Bhubaneswar, India*
[3]*Tolani Maritime Institute, Pune, India*
[4]*DRIEMS Autonomous Engineering College, Cuttack, India*
[5]*NIST Institute of Science and Technology, Berhampur, India*

Correspondence should be addressed to Murthy Cherukuri; chmurthy@nist.edu

Received 25 May 2023; Revised 10 July 2023; Accepted 31 August 2023; Published 12 September 2023

Academic Editor: Ricardo Caneloi dos Santos

In modern power systems, there is a greater penetration of renewable sources, resulting in the expansion of microgrid. By implementing RES instead of conventional synchronous machines, the system's overall inertia is significantly reduced. Modern and future power systems must reduce system inertia and keep the frequency at its nominal value since frequency oscillation impacts on the functionality, stability, and resilience of the system. Therefore, creating a stable, scalable, and reliable virtual inertia control system is crucial to effectively minimize the deviations during significant contingencies. Consequently, taking into account the probable issues, the foremost objective of this research work is to improve the dynamic security of an island microgrid through the implementation of a frequency control concept based on virtual inertia control. In the research study, the proposed microgrid system comprises of photovoltaics, wind-generating units, thermal power units, storage units, electric vehicles (EVs), and loads. A cascaded PIDFN controller is optimally designed using a novel metaheuristic modified differential evolution (MDE) algorithm that regulates the frequency based on virtual inertia control. In the MATLAB®/SIMULINK environment, various operating situations such as load variations, RES, and EVs disconnection are investigated, and the performance of the VIC-based MDE controller was compared to that of other controllers based on evolutionary optimization algorithms such as DE and TLBO. The results validate that the recommended virtual inertia control strategy enhances the reliability of the system.

1. Introduction

Recently, there has been a growing interest in integrating renewable energy sources (RESs) into electrical power grids as a future solution for reducing greenhouse gas emissions from conventional power plants, such as carbon dioxide and nitrogen oxide, which have negative environmental impacts. Consequently, a number of conventional generation units are being supplanted by distributed generators (DGs) and renewable energy sources (RES), such as solar energy, wind energy, microturbines, and small thermal power plants. In other words, modest sources of power generation, such as wind turbines and photovoltaic (PV), are connected to nearby distributed sites.

Although this concept has many advantages, such as the reduction of voltage droop and transmission system losses, and the improvement of system reliability, it has some negative effects on the performance of contemporary power systems, such as a lack of system inertia. In an isolated microgrid, virtual inertia is the concept of simulating the inertial response of synchronous generators using control techniques to enhance the microgrid's stability and frequency regulation during disturbances. Power electronic converters and energy storage systems are utilized to

simulate the operation of synchronous generators. The hypothesis applied to the system is to employ control strategies that simulate the inertia response of synchronous generators, which improves the frequency regulation and stability of an isolated microgrid during disturbances. Moreover, the efficacy and performance of these control methods may vary, and their implementation and fine-tuning in practice may necessitate careful consideration.

1.1. Literature Review. In recent years, the transformation from centralized to distributed power generation has made microgrids (MG) appealing and viable for incorporating renewable energy sources (RESs). The MG, comprising RESs, energy storage units, and loads, is an alternate solution for addressing energy shortages and environmental issues [1]. The sporadic nature of RESs leads to aberrant frequency oscillations in the power system that result in blackouts. Furthermore, the variation in required loads and the corresponding power mismatch between generation and load result in frequency variation and tie-line power fluctuation from their specified values. Consequently, load frequency control (LFC) has become integral to regulating stable and secure power system operation [2]. In literature, it has been observed that the frequency control in the power system consists of two loops. The primary loop makes up the inertia control and regulates the speed governor but does not regulate oscillations. The secondary loop mainly enables resolving frequency changes and tie-line power fluctuations across the power system [3]. In this regard, energy storage has evolved into an essential component for the reliable operation of MG. These storage units can adapt to load fluctuations and harness the system's additional electric power. The electric vehicle (EV) is gaining importance as it offers high energy density and continuous charging/discharging properties. Considering this, EVs are mostly employed for frequency regulation in MG due to the discrepancy between supply and demand and the stochastic nature of RES [4]. Additionally, EVs possess intrinsic benefits such as lower greenhouse emissions and the minimization of fossil fuel usage that have given an impetus to EVs [5].

Researchers have proposed various control strategies for the LFC analysis of an isolated MG incorporating EVs. In [6], authors have used conventional PI controllers, but these controllers failed to function effectively due to the stochastic nature of RES. Many researchers have implemented combinations of fractional order and conventional PID controllers [7], model predictive control [8], and sliding mode controllers [9] for load frequency analysis of standalone MG systems. Besides, Safiullah et al. [10] have suggested a robust frequency–voltage stabilization scheme for multi-area power systems incorporating electric vehicles (EVs) and renewable generations using an AI-based modified disturbance rejection controller. The proposed strategy mitigate disturbances in the power system, ensuring that the frequency and voltage remain within safe operating limits. Liu et al. [11] proposed an H-synthesis-based control strategy for mitigating the frequency deviation in an isolated MG. This approach being complicated, various optimization algorithms have been suggested by researchers, such as the genetic algorithm [12], squirrel search optimization [13], artificial bee colony algorithm [14], and differential evolution [15], to address the LFC problem of MG. Iqbal et al. [16] have proposed a synchronized strategy for regulating the frequency of implementing EVs under variable operating states, considering the cost of battery deterioration. Taking into consideration various charging profiles, the status of charge of electric vehicle batteries, and the number of electric vehicles in a fleet, two controllers (grid regulation and charger controller) are proposed. These controllers provide bidirectional power flow, which can provide primary frequency control during the various 24-hour contingencies, and an industrial microgrid may confront [17]. The proposed V2G strategy for primary frequency control is validated by applying a two-area interconnected industrial microgrid and another microgrid with renewable resources. In the proposed strategy, regulation specifications are communicated to electric vehicle and charging station operators via an electric vehicle aggregator. Currently, at the charging station operator, V2G power is used for frequency regulation capacity calculation [18]. Increasing penetration of renewable sources creates issues in the stability of microgrid. Loss of system inertia and damping is a major concern when replacing traditional generation units with RESs-based generation. The RESs are connected to the MG through a converter/inverter which results in the reduction of system inertia and damping that leads to system instability. In order to prevent system instability, inappropriate load, or generation shedding cascade outages and blackouts, it is necessary to maintain a considerable system inertia and damping generated by synchronous generators. Larger integration of RES reduces the system inertia and damping which has caused a major challenge in microgrid operation and control.

To overcome the stability issues of the MG, a virtual synchronous generator is proposed in [19] to improve the reliability and performance of the system. The notion of virtual inertia control (VIC) is evaluated as a distinct aspect of virtual synchronous machine (VSM) functioning that focuses on replicating the prime mover characteristics to generate inertia power for frequency stability. Integrating energy storage systems into the grid through inverters enables VIC by providing damping and inertia to conventional units. These strategies measure the rate of change in frequency and provide the necessary power to the MG, which further enhances stability [20]. In this regard, various control strategies such as H-infinite control [21], coefficient diagram [22], model predictive control [23], and fuzzy logic control [24] were implemented. The aforesaid controllers have several disadvantages, such as being complex in design, requiring more time for computational operation, and having a high cost. Various optimization strategies, such as particle swarm optimization [25] and genetic algorithms [26], were implemented to regulate the frequency of the microgrid. The solar negative resistance is greatly dependent on the solar operating temperature. At low irradiance, the system will become unresponsive and unstable. It is reported that the parallel impedance emulated condition (PIEC) nullifies the impact of negative solar resistance. During periods of low irradiance, system stability has shifted to an unstable state that cannot be resolved by PIEC. In this study,

a virtual inertia-damping voltage and current solar droop-emulated controller is proposed to enhance the DC microgrid system's voltage oscillation profile, inertia problem, and damping [27]. The conditions of series and parallel emulation that are highly dependent on negative resistance enhance voltage regulation. However, nonlinearities, inadequate damping, and inertia are inherent issues that make PV susceptible to instability and oscillations under varying irradiance. The virtual inertia feed-forward controller improved the oscillation problem and the initial notching of the PV system. However, the restoration controller minimizes the steady-state error of the PV voltage to ensure a stable system [28]. An innovative method was proposed for exploiting the virtual inertia potential of RES (photovoltaic systems) by cultivating the derivative control mechanism and enhancing the system's dynamic performance. In addition, the effectiveness of the proposed system is evaluated using time-domain simulations under varying conditions and compared to conventional and ESS-based systems [29].

The necessity to solve the difficulties of integrating renewable energy sources and ensure the system stability, frequency regulation, and optimal resource utilization in microgrid systems is the driving force behind the study on virtual inertia-based load frequency regulation in microgrids. In this context, by considering virtual inertia, a control and frequency control of the MG various optimization strategies are proposed in the literature. Considering the past observations made by researchers' rapid improvement of evolutionary algorithms has stimulated the development of a modified differential evolution algorithm in this study. This study suggests a novel design of cascaded PIDFN controller-based virtual inertia controller that is implemented to magnify the frequency of an isolated MG incorporating EV, photovoltaic, wind turbine, thermal power plant, and storage unit. The attributes of the controller are further modified using a modified differential evolution algorithm.

1.2. Research Contribution. The following goals are pursued by the research rationale, which addresses the frequency deviation control problem and the VIC application of islanded MGs based on an MDE-based PIDFN controller:

(1) A modified differential evolution algorithm that tunes the parameters of the cascaded PIDFN controller is presented

(2) The stability and resilience of an island microgrid are improved by using reliable virtual inertia controller-based MDE to reduce frequency variations, and a comparative study is carried out with other existing optimization algorithms such as DE and TLBO

(3) To evaluate the performance of the microgrid under various operating circumstances, disconnection of RESs, parametric variations, and load powers were taken into account

(4) The control method's resilience against the absence of EVs is evaluated

(5) To validate the stability analysis of the microgrid, the Eigenvalue technique is implemented

This study is organized as Section 2 represents the modelling of the interconnected microgrid system and the concept of virtual inertia control. The modified differential evolution algorithm is represented in Section 3. The simulation results and conclusion are represented in Section 4 and Section 5, respectively.

2. Modelling of Proposed System

A power system should maintain a generation-load balance since a mismatch between generation and load causes a large frequency deviation. This study examines an isolated MG to examine the efficacy of several frequency regulators. The main energy sources are conventional thermal units (TPP) and renewable energy sources, such as solar systems and wind turbine generator units (WTG) (PV). Electric vehicles (EVs), energy storage systems (ESUs), and loads are examples of consumer units and are illustrated in Figure 1.

The architecture of the isolated MG system governing frequency control is represented in

$$\Delta P_{TPP} + \Delta P_{PV} + \Delta P_{WTG} \pm \Delta P_{EV} \pm \Delta P_{ESS} - \Delta P_L = (Ms + D)\Delta f. \tag{1}$$

The objective function is the minimization of integral time absolute error (ITAE) of the frequency deviations of the system.

$$\text{ITAE} = \int_0^{t_s} |\Delta f|.t dt, \tag{2}$$

where t_s is the simulation time and Δf is the frequency deviation.

$$\begin{aligned} \text{Minimize ITAE}\left(K_p, K_i, K_d, N, K_{p1}, K_{i1}, u, K_{d1}, N_1, v_{11}\right), \\ 1 \le K_p \le 50, \\ 1 \le K_i \le 50, \\ 1 \le K_d \le 50, \\ 1 \le N \le 500, \\ 1 \le K_{p1} \le 50, \\ 1 \le K_{i1} \le 50, \\ 1 \le u \le 2, \\ 1 \le K_{d1} \le 50, \\ 1 \le N_1 \le 500, \\ 1 \le v_{11} \le 5. \end{aligned} \tag{3}$$

The objective function of ITSE, ISE, and IAE is also formulated in the same way.

The control dynamic equations that characterize every microgrid component are expressed as follows:

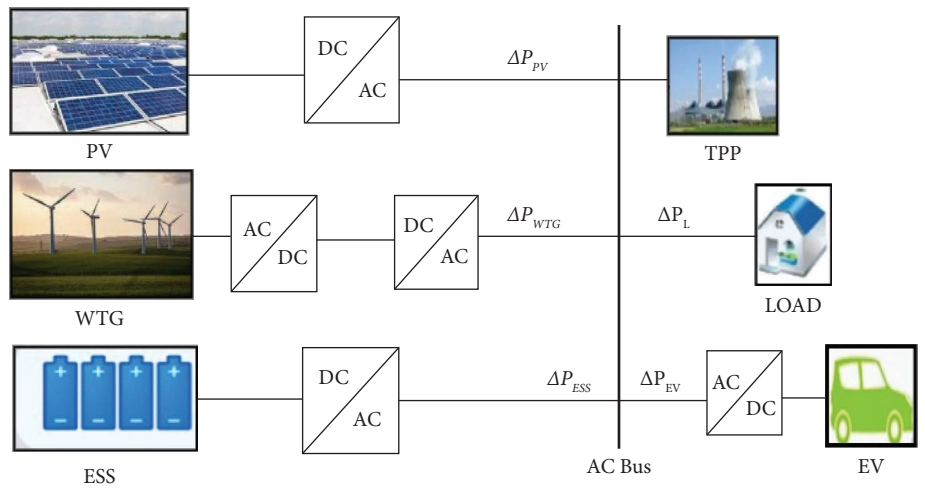

Figure 1: Proposed microgrid system.

$$\Delta P_{PV} = \frac{1}{1 + sT_{PV}}\Delta P_{\text{solar}},$$

$$\Delta P_{\text{WTG}} = \frac{1}{1 + sT_{\text{WTG}}}\Delta P_{\text{wind}},$$

$$\Delta P_{EV} = \frac{K_{EV}}{1 + sT_{EV}}\Delta f, \tag{4}$$

$$\Delta P_{ESS} = \frac{1}{1 + sT_{\text{ESS}}}.$$

2.1. Renewable Sources. Energy from the sun and wind is abundantly available across the globe and harnessed in terms of solar photovoltaic units (PV) and wind turbine generating units (WTG) that are used for generating power. PV units consist of an array of cells; the DC voltage is augmented by the converter, and the conversion into AC voltage is performed by the inverter that is utilized for generating electricity. The solar radiation, voltage, current, and temperature of PV cells determine the amount of generated PV energy [30]. The power extracted from the PV cells is determined by

$$P_{PV} = \eta S\phi\left(1 - 0.005\left(T_a + 25\right)\right), \tag{5}$$

where η = effectiveness of PV, S = surface area of PV, Φ = solar radiation intensity, and T_a = temperature of the surroundings.

In the WTG, the wind turbine propels the induction generator, which is further managed by the governor using the pitch angle of the turbine blade (β). The output power increment to the wind turbine generating (WTG) system is represented by the wind speed (V) and mechanical speed (ω) of the machine attached to the turbine. The output power (P_{wind}) represents the technical specifications as follows:

$$P_{\text{wind}} = 0.5\left(C_p\left(\lambda, \beta\right)A\eta\rho_a V^3\right), \tag{6}$$

where C_p is the capturing efficiency, λ is the ratio of tip speed, β is the wind turbine blade pitch, η is the efficiency, and ρ_a is the air density.

2.2. Thermal Power Plant. The fundamental steam model parameters, such as the time coefficient of the steam chest (T_{SC}), reheater (T_{RH})), crossover piping (T_{CO})), and the power fractions K_{HPT}, K_{IPT}, and K_{LPT}, affect how dynamically a steam turbine behaves. These power fractions represent the portions of the overall power produced by each pressure turbine (HPT, IPT, and LPT) [31].

2.3. Modelling of EV. Further functions to regulate EVs have been implemented to improve system efficiency with the significant substitution of predominant fossil fuel-powered vehicles by EVs. EV helps in stabilizing the frequencies that are caused by the variation of power from RES and power addressed by loads. They help to regulate the peak load, enhance the dependability of the grid, compensate for the influence of the sporadic nature of RES on grid fluctuations, and mitigate frequency instability by controlling the EV battery charging and discharging operations [32].

The EV offers the following advantages:

(a) They regulate the MG's frequency modulating their storage according to the system load variation

(b) It requires additional storage in MG that loads to consumption of additional energy storage system

(c) It also brings financial advantages to the owner by selling electricity at peak hours

In microgrids, electric vehicles (EVs) function as energy storage systems, allowing them to inject or ingest power to stabilize frequency. EVs monitor microgrid frequency using intelligent control algorithms and modify their power output accordingly, simulating the inertia response of conventional generators. They facilitate the virtual control of inertia and provide rapid response capabilities. By coordinating EV charging and discharging patterns, they can

respond to frequency variations by reducing demand during periods of high frequency and increasing charging capacity during periods of low frequency. EVs serve a crucial role in improving microgrid systems' stability, frequency regulation, and overall grid resilience. The power obtained from the EV is (ΔP_{EV}) which is the divergence of the regulation power (P_{EV}^{D}) and charging power (P_{EV}^{C}) of the EV.

$$\Delta P_{EV} = P_{EV}^{D} - P_{EV}^{C}. \tag{7}$$

2.4. Modelling of ESS. The energy storage system is one of the most ideal alternatives for providing frequency control in isolated MG due to its rapid reaction time and structural adaptability. An ultracapacitor is used, which is an electrostatic component that has a rapid response to power fluctuations represented by the transfer function as follows:

$$G_{\mathrm{ESS}}(s) = \frac{1}{1 + sT_{\mathrm{ESS}}}, \tag{8}$$

where T_{ESS} is the time constant of the energy storage unit.

2.5. Virtual Inertia Control of Microgrid. The main concern of microgrids is frequency stability, which occurs due to the disparity between the generated power and load consumption. The stored kinetic energy included in the pivoting mass of the synchronous generators provides inertia to the grid of conventional power systems. In the case of MG, the RESs replace the synchronous generators, which results in a lack of inertia due to the absence of rotating mass. This further degrades the stability and performance of the MG. Moreover, MG is vulnerable to large frequency distortions and short-circuit faults due to the absence of inertia [33]. The lack of inertia response can be mitigated by delivering active power emulated by a virtual inertia control strategy. This technique aims to replicate prime mover action in order to support the frequency stability of islanded MG. Based on derivative control, the virtual inertia control strategy reduces the active power of the islanded MG set point during high-level RES penetration and dependence and computes the rate of change of frequency.

In this study, energy storage units have been utilized to generate virtual inertia power, which simulates the kinetic energy stored in the rotating mass of a synchronous generator. According to Figure 2, the virtual inertia block is made up of a power limiter block, an inertia gain block, an energy storage component, and a derivative element.

The derivative control block forms the integral component as it evaluates the change in frequency, which supplies the required inertia power to the microgrid through energy storage units. The variation in frequency can be determined by using the following expression:

$$\text{Change in frequency} = \left[\frac{d}{dt}(\Delta f)\right]. \tag{9}$$

3. Modified Differential Evolution

In 1997, Storn et al. proposed the DE algorithm which was found to be superior as compared to other evolutionary algorithms in terms of simplicity, ease of implementation, and fewer variables. The DE algorithm operates in four phases, namely, initialization, mutation, crossover, and selection. In the first step, it starts with n numbers of population size and number of decision vectors distributed randomly as $\overrightarrow{\mathbf{X}_{\mathbf{k}}^{\mathbf{l}}} = (\mathbf{X}_{\mathbf{1}}^{\mathbf{l}}, \mathbf{X}_{\mathbf{2}}^{\mathbf{l}}, \ldots, \mathbf{X}_{\mathbf{D}}^{\mathbf{l}})$ over D-dimensional search space. In the second step, a mutant vector ($\overrightarrow{\mathbf{M}_{\mathbf{k}}^{\mathbf{l}}}$) is generated by applying the mutation operator to any of the following equations:

$$\text{DE/random/1: } \overrightarrow{M_k^1} = \overrightarrow{X_{k_1}^1} + f\left(\overrightarrow{X_{k_2}^1} - \overrightarrow{X_{k_3}^1}\right), \tag{10}$$

$$\text{DE/ideal/1: } \overrightarrow{M_k^1} = \overrightarrow{X_{\mathrm{best}}^1} + f\left(\overrightarrow{X_{k_1}^1} - \overrightarrow{X_{k_2}^1}\right), \tag{11}$$

$$\text{DE/random/2: } \overrightarrow{M_k^1} = \overrightarrow{X_{k_5}^1} + f\left(\overrightarrow{X_{k_1}^1} - \overrightarrow{X_{k_2}^1}\right) + f\left(\overrightarrow{X_{k_3}^1} - \overrightarrow{X_{k_4}^1}\right), \tag{12}$$

$$\text{DE/ideal/2: } \overrightarrow{M_k^1} = \overrightarrow{X_{\mathrm{best}}^1} + f\left(\overrightarrow{X_{k_1}^1} - \overrightarrow{X_{k_2}^1}\right) + f\left(\overrightarrow{X_{k_3}^1} - \overrightarrow{X_{k_4}^1}\right), \tag{13}$$

$$\text{DE/current} - \text{to} - \text{ideal/1: } \overrightarrow{M_k^1} = \overrightarrow{X_k^1} + f\left(\overrightarrow{X_{\mathrm{best}}^1} - \overrightarrow{X_k^1}\right) + f\left(\overrightarrow{X_{\mathrm{best}}^1} - \overrightarrow{X_{k_2}^1}\right). \tag{14}$$

In the third step, the decision vector ($\overrightarrow{X_k^l}$) and mutant vector ($\overrightarrow{M_k^l}$) undergo crossover operation to form a trial vector (V_{ij}^l), expressed as follows:

$$V_{kj}^{l} = \begin{cases} M_{kj}^{l}, \text{ if r and } (0,1) < Cr, \\ X_{kj}^{l}, \text{otherwise,} \end{cases} \quad \text{for } j = 1, 2, \cdots, D. \tag{15}$$

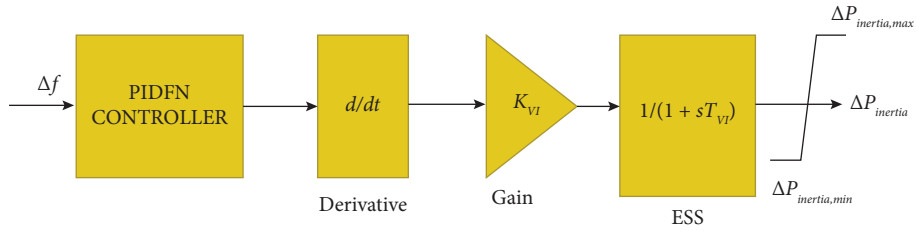

Figure 2: Virtual inertia block.

In the last step, the vector for the next generation is selected as per the following expression:

$$X_k^{l+1} = \begin{cases} V_k^l, & \text{if fitness of } V_k^l \text{ is better than } X_k^l, \\ X_k^l, & \text{otherwise,} \end{cases} \quad (16)$$

where $\overrightarrow{X_k^l}$ is the kth decision vector of lth generation, $\overrightarrow{M_k^l}$ is the kth mutant vector of lth generation, $\overrightarrow{X_k^l}$ and $\overrightarrow{X_{\text{best}}^l}$ are the lth generation's randomly chosen decision vector and best solution vector, respectively, f is the scale factor, and Cr is the crossover rate whose value ranges between 0 and 1. In this work, f and Cr are chosen 0.5 and 0.6, respectively.

The mutation operator like the DE/rand mutation operator has more exploration features than exploitation which also takes more time to attain optimal solutions. Similarly, the DE/best mutation operator has more exploitation features than exploration and takes less time to obtain the optimal solution. This approach, however, suffers from early convergence and being stuck in local optima. A novel mutation operator is presented in the MDE algorithm to prevent the above difficulty and maintain a balance between exploitation and exploration [34]. Here, six best solutions from the current generation are chosen to find three mutant vectors (17)–(19). The final mutant vector ($\overrightarrow{M_k^l}$) is then determined by taking the average of these three mutant vectors. In crossover step, a new trial vector is obtained as per (20). Finally, in the selection step, the decision vector for the next generation is obtained as expressed in equation (21).

$$\overrightarrow{M_1} = \overrightarrow{X_k^l} + f\left(\overrightarrow{X_{\text{best1}}^l} - \overrightarrow{X_k^l}\right) + f\left(\overrightarrow{X_{\text{best2}}^l} - \overrightarrow{X_k^l}\right), \quad (17)$$

$$\overrightarrow{M_2} = \overrightarrow{X_k^l} + f\left(\overrightarrow{X_{\text{best}_3}^l} - \overrightarrow{X_k^l}\right) + f\left(\overrightarrow{X_{\text{best4}}^l} - \overrightarrow{X_k^l}\right), \quad (18)$$

$$\overrightarrow{M_3} = \overrightarrow{X_k^l} + f\left(\overrightarrow{X_{\text{best5}}^l} - \overrightarrow{X_k^l}\right) + f\left(\overrightarrow{X_{\text{best6}}^l} - \overrightarrow{X_k^l}\right), \quad (19)$$

$$\overrightarrow{M_k^l} = \text{Mean}\left(\overrightarrow{M_1}, \overrightarrow{M_2}, \overrightarrow{M_3}\right), \quad (20)$$

$$f = 2 \times \left(1 - \frac{l}{L_{\max}}\right), \quad (21)$$

where $\overrightarrow{X}_{\text{best1}}^l$, $\overrightarrow{X}_{\text{best2}}^l$, $\overrightarrow{X}_{\text{best3}}^l$, $\overrightarrow{X}_{\text{best4}}^l$, $\overrightarrow{X}_{\text{best5}}^l$, and $\overrightarrow{X}_{\text{best6}}^i$ are the six best decision vectors chosen from lth generation. l and $L_{\max}$ are the current and maximum generation, respectively. Figure 3 shows the flowchart of the MDE algorithm.

The robustness of the proposed method is validated on different benchmark functions. The results are obtained considering 500 iterations and 10 repetitions. The comparison is analyzed among TLBO, DE, and MDE and depicted in Table 1.

4. Results and Discussion

In this article, the significance of implementing an MDE-PIDFN-based virtual inertia controller to minimize the frequency fluctuations is addressed. The PIDFN controller [35] parameters are tuned using a modified differential evolution algorithm. The proposed microgrid regulates the frequency and time deviation within the specified limits which is validated using four test scenarios. The size of the population, swarm size, and number of search agents are set at 20 up to 100 iterations. The design of objective functions is used to adjust the controller parameters that are based on performance indices that account for frequency response. The optimization algorithms are measured in terms of performance indices: integral square error (ISE), integral absolute error (IAE), integral time square error (ITSE), and integral time absolute error (ITAE).

4.1. Effect of Step Load. In this scenario, the impact of VIC-MDE in minimizing frequency fluctuations in area 1 is investigated by 1% change in step load. Figure 4 demonstrates that the VIC-MDE controller enhances the frequency performance and transient disturbances as compared to VIC-DE- and VIC-TLBO-based controllers.

From Figure 4, it is found that the VIC-MDE controller has a better performance and achieves a better settling time in comparison to additional controllers. The results of the various controllers are implemented as outlined in Table 2.

Table 2 reflects that the proposed VIC-MDE has the lowest performance indicator value as compared to other controllers. Moreover, the proposed controller improves the PUS by 50% and 10% as compared to VIC-TLBO and VIC-DE controllers, respectively.

4.2. Effect of Variable Load. In this scenario, the tuning of cascaded PIDFN-based virtual inertia controller by MDE under variable load disturbance is introduced. The suggested microgrid was subjected to real-time variations of solar irradiance and wind speed collected from a local plant. The system is subjected to real-time variation of solar irradiance and wind speed and subjected to variable load as shown in Figure 5.

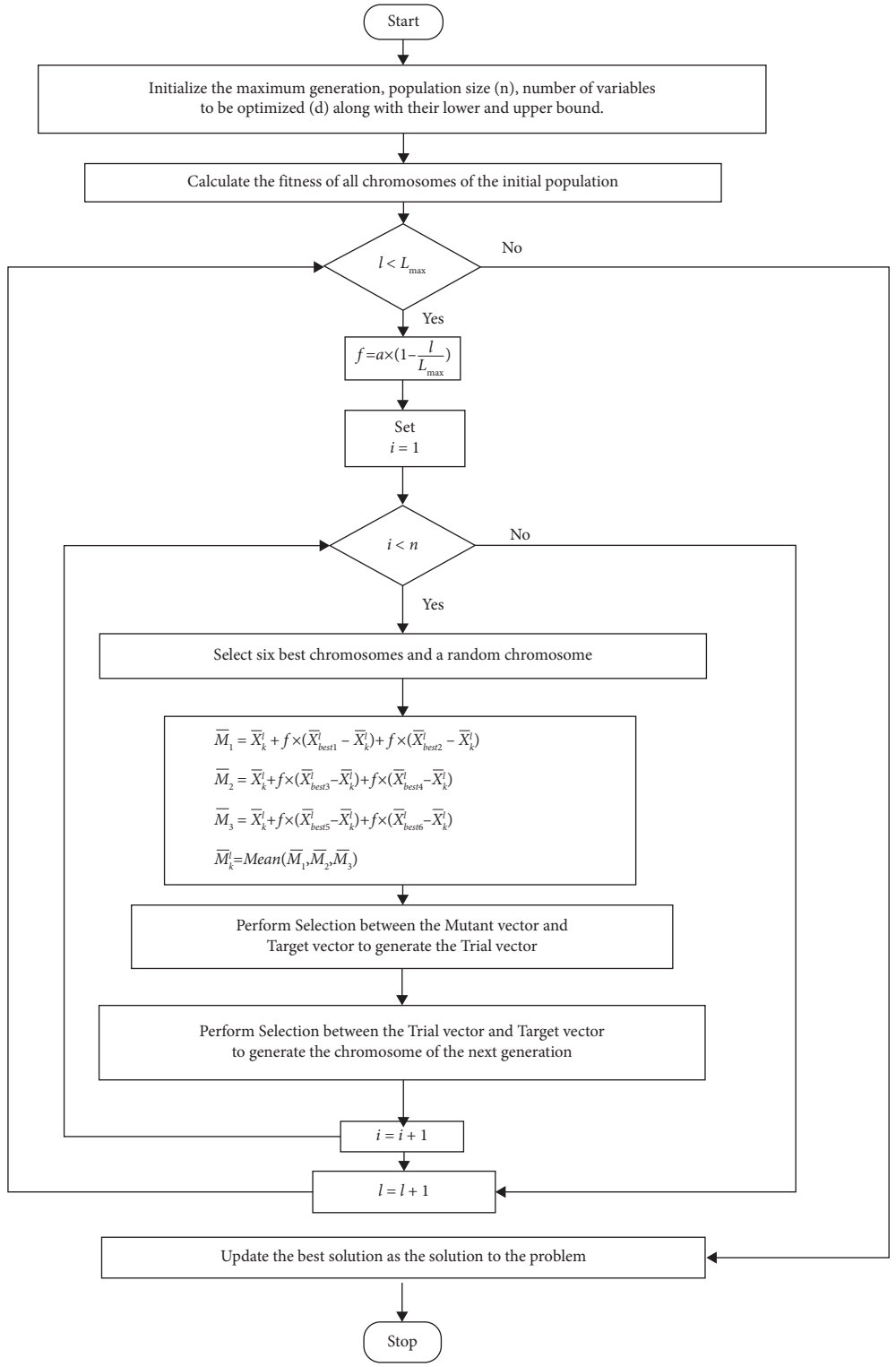

Figure 3: Flowchart of MDE.

From Figure 6, it is analyzed that the suggested controller has a better performance and minimizes frequency disruptions effectively as compared to other controllers. The performance and the transient specifications of various controllers are represented in Table 3.

From Table 3, it has been noted that the VIC-MDE controller has a better fitness value as compared to VIC-DE and VIC-TLBO controllers. The proposed VIC-MDE algorithm outperforms and has sustained oscillations and improves the PUS by 81.08% and 72% as compared to other controllers.

Table 1: Statistical analysis of the proposed method on benchmark functions.

Functions	Methods	Best	Worst	Mean	SD
F_1	MDE	$4.68E-21$	$7.36E-19$	$7.41E-20$	$1.85E-19$
	DE	$6.78E-22$	$1.19E-14$	$2.39E-16$	$1.67E-15$
	TLBO	$1.44E-91$	$3.38E-89$	$1.26E-89$	$1.10884E-89$
F_2	MDE	$2.58E-21$	$2.27E-16$	$3.32E-17$	$7.12E-17$
	DE	$8.38E-13$	$1.72E-11$	$4.46E-12$	$3.42E-12$
	TLBO	$2.49E-44$	$2.13E-43$	$1.00E-43$	$6.02063E-44$
F_3	MDE	$1.80E-05$	0.013169	0.00188	0.00303
	DE	0.000615	0.532483	0.049855	0.090053
	TLBO	$1.77E-20$	$2.74E-16$	$3.63E-17$	$8.02234E-17$
F_4	MDE	$7.57E-06$	6.2443	0.64133	1.6845
	DE	$5.73E-06$	15.27477	0.867372	2.910621
	TLBO	$1.88E-37$	$2.06E-36$	$1.30E-36$	$5.88547E-37$
F_5	MDE	0.0001369	0.22622	0.17203	0.12704
	DE	0.08269	21.13767	6.189471	2.75689
	TLBO	24.62261	25.73328	25.14059	0.36851
F_6	MDE	$3.537E-24$	$4.049E-20$	$2.2988E-20$	$3.53592E-20$
	DE	$7.79E-22$	$7.83E-19$	$8.74E-20$	$1.56E-19$
	TLBO	$1.32E-07$	$7.44E-05$	$1.64E-05$	$2.35864E-05$
F_7	MDE	0.0013	0.00757	0.0037	0.0018
	DE	0.000761	0.018048	0.005162	0.002945
	TLBO	0.000543	0.001908	0.001354	0.000389
F_8	MDE	−4189.83	−3634.99	−3902.1344	158.86
	DE	−4079.23	−3558.16	−3847.11	202.5658
	TLBO	−1670.31	−1468.19	−1556.2	64.26864
F_9	MDE	1.99	12.93	6.89	3.06
	DE	4.10	13.72706	8.052266	3.152745
	TLBO	9.061606	14.9362	12.07996	1.600468
F_{10}	MDE	$2.075E-12$	$1.019E-10$	$3.562E-11$	$3.803E-11$
	DE	$1.98E-11$	$4.55E-10$	$1.22E-10$	$7.89E-11$
	TLBO	19.99999996	20	19.99999996	$1.45389E-09$
F_{11}	MDE	$9.554E-06$	0.16982	0.055	0.054
	DE	$1.11E-16$	0.271709	0.069238	0.069303
	TLBO	0	0	0	0
F_{12}	MDE	$1.58E-26$	$3.81E-21$	$4.294E-22$	$1.052E-21$
	DE	$1.11E-22$	0.29231	0.005846	0.040923
	TLBO	$4.21E-09$	$1.40E-06$	$2.43E-07$	$3.98225E-07$
F_{13}	MDE	$1.2315E-21$	$9.78E-20$	$2.46E-20$	$2.65E-20$
	DE	$1.51E-21$	$5.75E-19$	$3.92E-20$	$8.74E-20$
	TLBO	$1.151E-05$	0.206965	0.084465	0.068102

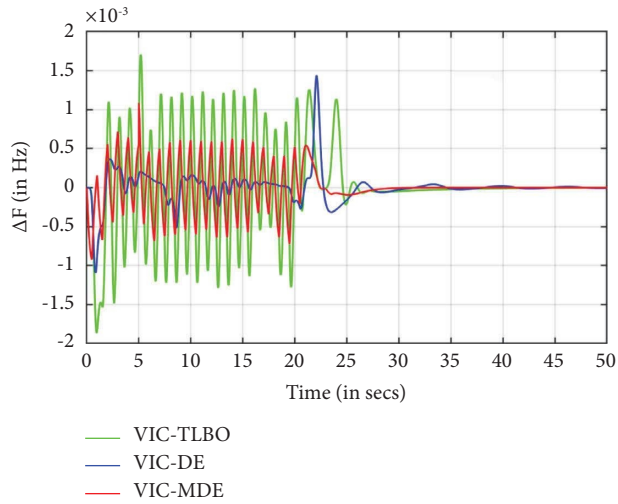

Figure 4: Frequency deviation under step load variation.

Table 2: Performance metrics under step load.

Performance criterion	VIC-TLBO	VIC-DE	VIC-MDE
ISE	$1.61E-03$	$1.83E-07$	$1.45E-07$
IAE	0.0014919	0.00072905	0.00072064
ITSE	0.0014801	0.000342	0.0000123
ITAE	0.00162	0.0014499	0.0012243
PUS (Hz)	0.0018	0.0010	0.0009
TS (secs)	Unstable	32.34	31.22

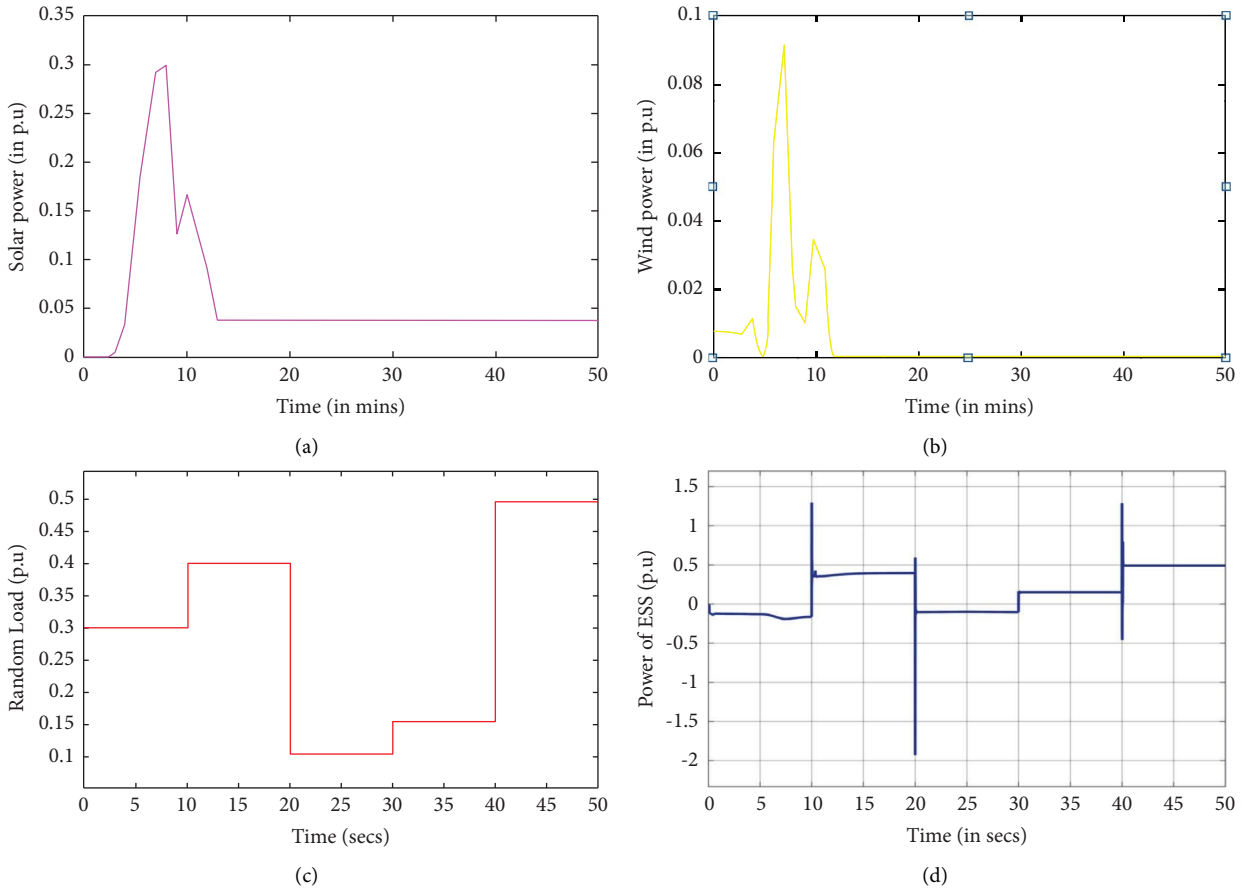

Figure 5: (a) Variation in solar power. (b) Variation in wind power. (c) Variation in load profile. (d) Power of ESS.

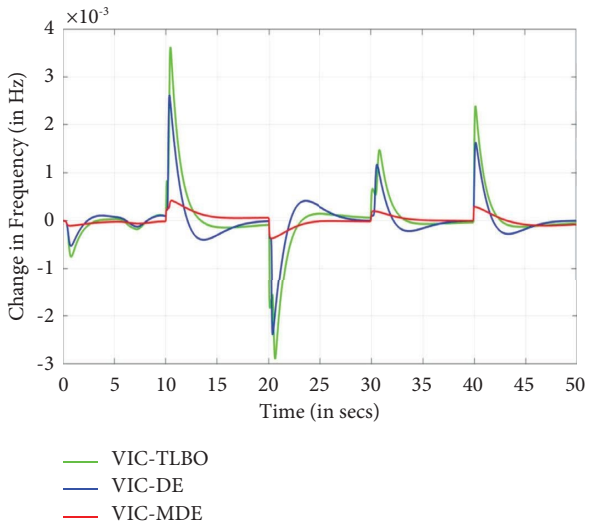

Figure 6: Frequency variation under random load variations.

Table 3: Performance metrics under variable load.

Performance criterion	VIC-TLBO	VIC-DE	VIC-MDE
ISE	$1.41E-03$	$2.14E-07$	$1.28E-07$
IAE	0.0011357	0.0014149	0.00074427
ITSE	0.001419	0.000109	0.000065
ITAE	0.00475	0.00375	0.00173
PUS (Hz)	0.00074	0.0005	0.00014
TS (secs)	Oscillatory	Oscillatory	Stable

4.3. Parameter Variation. The behavior of the microgrid is evaluated under extreme conditions where the generation constant of turbine and thermal is increased to $T_g = 0.12$ sec and $T_t = 0.975$ sec, respectively. This situation might arise as a result of off-line changes to the turbine and governor parameters. Moreover, the damping coefficient value is raised to $D = 0.0195$ (p.u. MW/Hz), which is a 35% increase beyond its nominal value and system inertia falls to 30% of its nominal value, which is a key condition as this leads to unstable situation of thermal power plant and microgrid. Figure 7 shows the microgrid frequency variation in the case of parametric variations.

From Figure 7, it is analyzed that the proposed controller modulates the frequency of the system frequency within its specified values as compared to other controllers. The values of various controllers are demonstrated in Table 4.

In this scenario, it has been adequately proved that the reaction of the MG with the recommended control technique is more useful and efficient than utilizing alternative controllers. The settling time is improved by 14.25% and is stable as compared to other controllers.

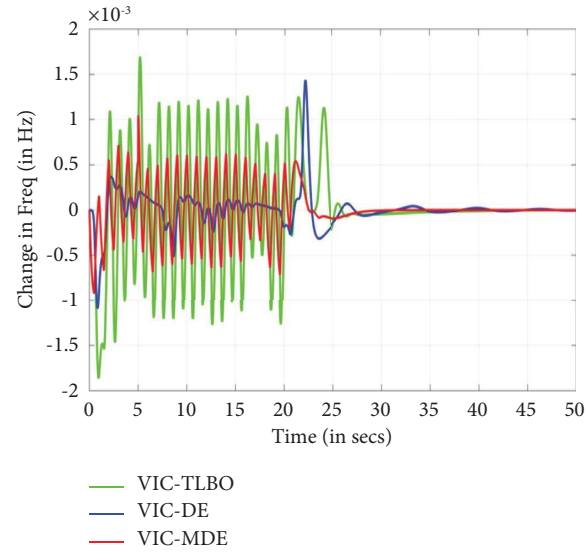

Figure 7: Frequency variation under parameter variations.

4.4. RES Disconnection. In this scenario, RES is disconnected, and the performance of the controllers is assessed to measure the efficacy of the proposed controller. The solar panels are disconnected at 30 seconds, and their impact on the performance of the various controllers is represented in Figure 8.

Figure 8 clearly demonstrates that the suggested controller has a better performance in contrast to other controllers. The proposed VIC-MDE-based controller has sustained oscillations and has a better efficacy. The transient specifications are presented in Table 5.

From Table 4, it is observed that the proposed VIC-MDE controller has sustained oscillations and has an improved undershoot and settling time performance and better indices. The settling time is further enhanced by 21% and 6.4% as compared to VIC-TLBO and VIC-DE controllers.

Table 4: Performance metrics under parameter variations.

Performance criterion	VIC-TLBO	VIC-DE	VIC-MDE
ISE	$1.41E-03$	$3.54E-06$	$1.80E-07$
IAE	0.0014149	0.007799	0.0007558
ITSE	0.004113	0.003410	0.0014149
ITAE	0.00657	0.00741	0.00107
PUS (Hz)	0.00185	0.0010	0.00087
TS (secs)	35	Oscillatory	30

4.5. Absence of EV. An incessant step load disturbance/demand is projected to the area in the absence of EVs to test the resilience of the suggested VIC-MDE controller. EVs are utilized in power system frequency regulation problem resolution by supplying active power to load or requesting additional active power from generation, and EVs will quickly compensate for the active power gap between demand and generation, hence enhancing the frequency stability or load frequency control of the power system. The performance of the system in the absence of EVs is represented in Figure 9.

Figure 9 clearly demonstrates that the suggested controller has a better performance in contrast to other controllers in the absence of EVS. The transient specifications are presented in Table 6.

From the previous figure, it depicts that the proposed controller has a better performance as compared to other controllers. The PUS is improved by 50.5% and 15.23% as compared to VIC-TLBO and VIC-DE controllers.

The controller parameters of the controllers under different scenarios are represented in Table 7.

4.6. Stability Analysis by Eigenvalues. The eigenvalues analysis strategy is used to assess the system's stability. Eigenvalues are analyzed in order to determine the stability of

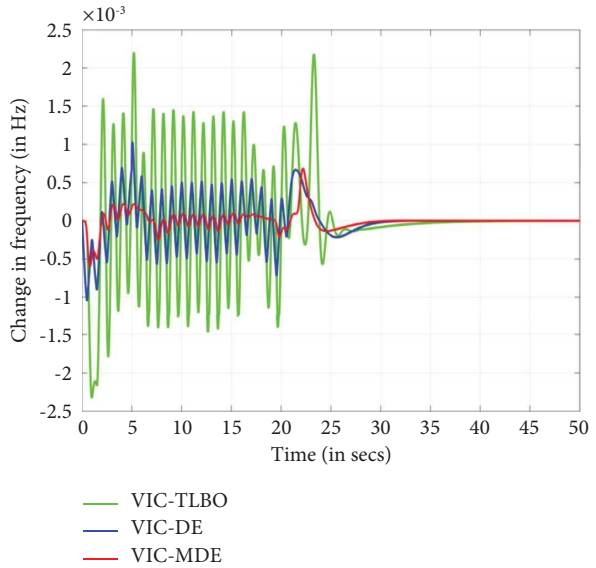

Figure 8: Frequency fluctuation due to RES.

Table 5: Performance metrics under RES disconnection.

Performance criterion	VIC-TLBO	VIC-DE	VIC-MDE
ISE	$2.57E-05$	$3.6E-06$	$8.01E-07$
IAE	0.022	0.00803	0.003251
ITSE	0.02795	0.0089	0.00405
ITAE	0.00761	0.00876	0.00089
PUS (Hz)	0.0023	0.0010	0.00057
TS (secs)	37	31	29

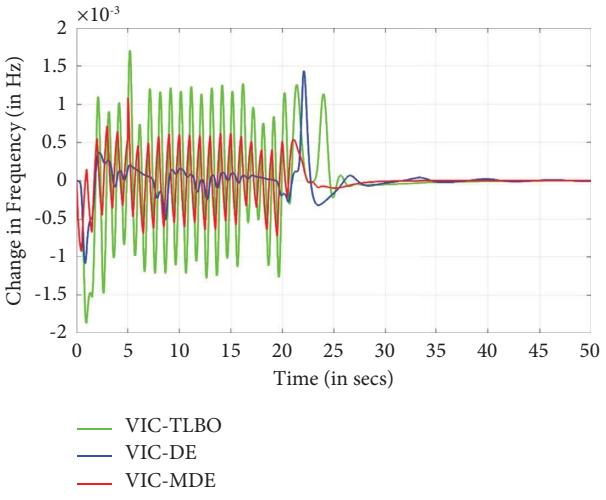

Figure 9: Frequency fluctuation due to the absence of EVs.

Table 6: Performance metrics under the absence of EVs.

Performance criterion	VIC-TLBO	VIC-DE	VIC-MDE
ISE	$1.63E-05$	$3.09E-06$	$2.09E-06$
IAE	0.01752	0.005105	0.005005
ITSE	$4.06E-03$	$2.983E-05$	$7.37E-06$
ITAE	0.2102	0.872	0.739
PUS (Hz)	0.0018	0.00105	0.00089
TS (secs)	39	38	35

Table 7: Controller parameters.

Cases	Controllers	K_P	K_I	K_D	N	K_{P1}	K_{I1}	U	K_{D1}	N_1	V_{11}
I	VIC-TLBO	3.4488	50	2.6022	12.1541	44.0624	6.4548	1.087	50	500	3.6356
	VIC-DE	49.3887	49.8865	25	1	9.9844	49.7619	1	15	264.983	3.4513
	VIC-MDE	49.79	50	1	44.923	7.8733	50	1	18.228	120.123	3.63
II	VIC-TLBO	49.9762	49.99	1.1383	498.9891	49.1156	9.856	1.0062	49.9629	100.703	49.99
	VIC-DE	50	50	23.521	1	50	31.8719	1	50	102.841	5
	VIC-MDE	50	50	37.5915	1	258.9103	34.5455	3.8857	23	438.9103	5
III	VIC-TLBO	3.4488	50	2.6022	12.1541	44.0624	6.4548	1.0582	50	500	3.6356
	VIC-DE	49.3887	49.8865	25	1	9.9844	49.7619	1	15	264.983	3.4513
	VIC-MDE	49.79	50	1	44.923	7.8733	50	1	18.118	1	3.63
IV	VIC-TLBO	3.4488	50	2.6022	12.1541	32.99	7.292	1.0897	50	500	3.6356
	VIC-DE	49.3887	49.8865	25	1	29.9844	49.7619	1	15	264.983	3.4513
	VIC-MDE	40.79	45	2	44.923	19.82	25	1	18.118	1	1.92
V	VIC-TLBO	3.4488	50	2.6022	12.1541	44.0624	6.4548	1.087	50	500	3.6356
	VIC-DE	49.3887	49.8865	25	1	9.9844	49.7619	1	15	264.983	3.4513
	VIC-MDE	49.79	50	1	44.923	7.8733	50	1	1	18.118	3.63

Table 8: Eigenvalues of various controllers.

Controllers	Eigenvalues		
VIC-TLBO	$-3.33e+01$	$-8.33e+00$	$-1.33e+00+3.95e+00$
	$-5.00e+00$	$-3.34e+00$	$-9.46e-05$
	$-2.50e+00$	$1.70e-14+2.00e-09i$	$-3.32e-11$
	$-6.67e+01$		
VIC-DE	$-3.34e+00$	$-2.50e+00$	$-6.67e-01+4.75e-01$
	$-2.00e-01$	$-1.25e-02$	$-1.47e-10$
	$-6.67e-01$		
VIC-MDE	$-5.00e+00$	$-3.34e+00$	$-7.08e-14$
	$-1.90e+00$	$-1.03e+00$	$-2.00e+01$
	$-5.53e+09$		

the proposed TLBO, DE, and MDE-based virtual inertia cascaded controllers. The eigenvalues are estimated in accordance with the linmod function which is displayed in Table 8. The fact that all eigenvalues have negative real components, as shown in Table 8, confirms that the system is stable with adequate stability margins. The minimal magnitude of the imaginary component of the eigenvalues indicates the quick decay of system responsiveness. Hence, the performed study demonstrates that the proposed controller has increased the system's stability.

5. Conclusions

Frequency instability in the microgrid arises due to larger penetration of renewable energy resources that result in the reduction of inertia. In this research paper, a novel VIC-MDE controller is proposed. The parameters of the controller are optimized using the MDE technique. In order to compare the VIC-MDE controller performance with that of other optimization methods, such as DE and TLBO, various test scenarios such as the disconnections of RESs, load power fluctuations, and system uncertainties are taken into account. It is observed that when the system is subjected to load variations, the proposed VIC-MDE controller improves the PUS by 81% and 72% as compared to VIC-TLBO and VIC-DE controllers. Similarly, during disconnection of RES, the PUS is improved by 75% and 43%, and settling time is improved by 21% and 7% using the VIC-MDE controller. The above results validate the supremacy of the proposed VIC-MDE controller as compared to VIC-TLBO and VIC-DE controllers. The suggested controller is accountable for maintaining frequency variation and stabilizing the power system by decreasing peak undershoot and oscillations.

Data Availability

The data supporting the current study are available from the corresponding author upon request.

Conflicts of Interest

The authors declare that they have no conflicts of interest.

References

[1] I. Todorović, I. Isakov, D. Reljić, D. G. Jerkan, and D. Dujić, "Mitigation of voltage and frequency excursions in low-inertia microgrids," *IEEE Access*, vol. 11, pp. 9351–9367, 2023.

[2] E. Bahrampour, M. Dehghani, M. H. Asemani, and R. Abolpour, "Load frequency fractional-order controller design for shipboard microgrids using direct search

alghorithm," *IET Renewable Power Generation*, vol. 17, no. 4, pp. 894–906, 2023.

[3] R. Kumar Khadanga, A. Kumar, and S. Panda, "Frequency control in hybrid distributed power systems via type-2 fuzzy PID controller," *IET Renewable Power Generation*, vol. 15, no. 8, pp. 1706–1723, 2021.

[4] F. Tao, L. Zhu, Z. Fu, P. Si, and L. Sun, "Frequency decoupling-based energy management strategy for fuel cell/battery/ultracapacitor hybrid vehicle using fuzzy control method," *IEEE Access*, vol. 8, pp. 166491–166502, 2020.

[5] M. Elsisi, M. Soliman, M. A. Aboelela, and W. Mansour, "Model predictive control of plug-in hybrid electric vehicles for frequency regulation in a smart grid," *IET Generation, Transmission & Distribution*, vol. 11, no. 16, pp. 3974–3983, 2017.

[6] Y. Arya, "Effect of electric vehicles on load frequency control in interconnected thermal and hydrothermal power systems utilising CF-FOIDF controller," *IET Generation, Transmission & Distribution*, vol. 14, no. 14, pp. 2666–2675, 2020.

[7] A. Prakash, K. Kumar, and S. K. Parida, "PIDF(1+FOD) controller for load frequency control with SSSC and AC–DC tie-line in deregulated environment," *IET Generation, Transmission & Distribution*, vol. 14, no. 14, pp. 2751–2762, 2020.

[8] S. Kayalvizhi and D. M. Vinod Kumar, "Load frequency control of an isolated micro grid using fuzzy adaptive model predictive control," *IEEE Access*, vol. 5, pp. 16241–16251, 2017.

[9] X. Lv, Y. Sun, S. Cao, and V. Dinavahi, "Event-triggered load frequency control for multi-area power systems based on Markov model: a global sliding mode control approach," *IET Generation, Transmission & Distribution*, vol. 14, no. 21, pp. 4878–4887, 2020.

[10] S. Safiullah, A. Rahman, S. A. Lone, S. S. Hussain, and T. S. Ustun, "Robust frequency–voltage stabilization scheme for multi-area power systems incorporated with EVs and renewable generations using AI based modified disturbance rejection controller," *Energy Reports*, vol. 8, pp. 12186–12202, Nov. 2022.

[11] T. Liu, A. Chen, F. Gao, X. Liu, X. Li, and S. Hu, "Double-loop control strategy with cascaded model predictive control to improve frequency regulation for islanded microgrids," *IEEE Transactions on Smart Grid*, vol. 13, no. 5, pp. 3954–3967, Sep. 2022.

[12] D. Zhang, "Multi-objective control of residential HVAC loads for balancing the user's comfort with the frequency regulation performance," *IEEE Transactions on Smart Grid*, vol. 13, no. 5, pp. 3546–3557, Sep. 2022.

[13] G. Dei, "Improved squirrel search algorithm driven cascaded 2DOF-PID-FOI controller for load frequency control of renewable energy based hybrid power system," *IEEE Access*, vol. 10, pp. 46372–46391, 2022.

[14] M.-T. Kuo, "Application of the artificial bee colony algorithm to scheduling strategies for energy-storage systems of a microgrid with self-healing functions," *IEEE Transactions on Industry Applications*, vol. 57, no. 3, pp. 2156–2167, May 2021.

[15] L. Kumar, M. K. Kar, and S. Kumar, "Reactive power management of transmission network using evolutionary techniques," *Journal of Electrical Engineering & Technology*, vol. 18, no. 1, pp. 123–145, 2023.

[16] S. Iqbal, S. Habib, N. H. Khan, M. Ali, M. Aurangzeb, and E. M. Ahmed, "Electric vehicles aggregation for frequency control of microgrid under various operation conditions using an optimal coordinated strategy," *Sustainability*, vol. 14, no. 5, p. 3108, 2022.

[17] S. Iqbal, "Aggregation of EVs for primary frequency control of an industrial microgrid by implementing grid regulation & charger controller," *IEEE Access*, vol. 8, pp. 141977–141989, 2020.

[18] S. Iqbal, "V2G strategy for primary frequency control of an industrial microgrid considering the charging station operator," *Electronics*, vol. 9, no. 4, p. 549, 2020.

[19] D. Mishra, M. K. Maharana, M. K. Kar, and A. Nayak, "Frequency management of an interconnected power system using modified differential evolution algorithm," *International Journal of Renewable Energy Resources*, vol. 13, no. 2, pp. 515–525, 2023.

[20] A. Fathi, Q. Shafiee, and H. Bevrani, "Robust frequency control of microgrids using an extended virtual synchronous generator," *IEEE Transactions on Power Systems*, vol. 33, no. 6, pp. 6289–6297, 2018.

[21] V. Skiparev, R. Machlev, N. R. Chowdhury, Y. Levron, E. Petlenkov, and J. Belikov, "Virtual inertia control methods in islanded microgrids," *Energies*, vol. 14, no. 6, p. 1562, 2021.

[22] T. Kerdphol, M. Watanabe, K. Hongesombut, and Y. Mitani, "Self-adaptive virtual inertia control-based fuzzy logic to improve frequency stability of microgrid with high renewable penetration," *IEEE Access*, vol. 7, pp. 76071–76083, 2019.

[23] H. Ali, "A new frequency control strategy in an islanded microgrid using virtual inertia control-based coefficient diagram method," *IEEE Access*, vol. 7, pp. 16979–16990, 2019.

[24] R. Mandal and K. Chatterjee, "Virtual inertia emulation and RoCoF control of a microgrid with high renewable power penetration," *Electric Power Systems Research*, vol. 194, pp. 1–12, 2021.

[25] J. Sun, M. Chen, L. Kong, Z. Hu, and V. Veerasamy, "Regional load frequency control of BP-PI wind power generation based on particle swarm optimization," *Energies*, vol. 16, no. 4, p. 2015, 2023.

[26] K. Anuradhika and P. Dash, "Genetic algorithm-based load frequency control of a grid-connected microgrid in presence of electric vehicles," in *Sustainable Energy and Technological Advancements: Proceedings of ISSETA 2021*, pp. 435–447, Springer, New York, NY, USA, 2022.

[27] M. R. Yadav and N. Singh, "Impact of negative solar resistance on DC microgrid stability: virtual damping voltage and current solar droop emulated controller," *J CIRCUIT SYST COMP*, vol. 32, no. 08, Article ID 2350126, 2023.

[28] M. Yadav and N. Singh, "Impact of variable negative solar resistance: modified virtual feed forwarded with feedback emulated inertia controller," *International Journal of Ambient Energy*, vol. 43, no. 1, pp. 6511–6523, Dec. 2022.

[29] P. Saxena, N. Singh, and A. K. Pandey, "Enhancing the dynamic performance of microgrid using derivative controlled solar and energy storage based virtual inertia system," *Journal of Energy Storage*, vol. 31, Article ID 101613, 2020.

[30] M. Al-Saadi, E. A. Hussien, and A. Craciunescu, "Maximum power point tracking and power/voltage regulation for inductive wireless battery charging," in *Proceedings of the 2019 Electric Vehicles International Conference (EV)*, pp. 1–6, New York, NY, USA, August 2019.

[31] A. Nayak, M. K. Maharana, T. Sidhu, S. Padmanaban, and G. Panda, "Frequency regulation of a maiden structured power system with integrated renewable energy source by a fuzzy-tuned fractional order controller," *Energy Sources, Part A: Recovery, Utilization, and Environmental Effects*, vol. 44, no. 3, pp. 7841–7856, 2022.

[32] P. C. Sahu, R. C. Prusty, and S. Panda, "Frequency regulation of an electric vehicle-operated micro-grid under WOA-tuned

fuzzy cascade controller," *International Journal of Ambient Energy*, vol. 43, no. 1, pp. 2900–2911, 2022.

[33] A. Saleh, W. A. Omran, H. M. Hasanien, M. Tostado-Véliz, A. Alkuhayli, and F. Jurado, "Manta ray foraging optimization for the virtual inertia control of islanded microgrids including renewable energy sources," *Sustainability*, vol. 14, no. 7, p. 4189, 2022.

[34] D. Mishra, M. K. Maharana, M. K. Kar, and A. Nayak, "A modified differential evolution algorithm for frequency management of interconnected hybrid renewable system," *International Journal of Power Electronics and Drive Systems*, vol. 14, no. 3, pp. 1711–1721, 2023.

[35] D. Mishra, M. K. Maharana, and A. Nayak, "Frequency amelioration of an interconnected microgrid system," *Open Engineering*, vol. 12, no. 1, pp. 349–358, 2022.